HIGH-EFFICIENCY AMORPHOUS SILICON ALLOY BASED SOLAR CELLS AND MODULES

Quarterly Technical Progress Report
September 1, 2004 through November 30, 2004

S. Guha and J. Yang
United Solar Ovonic Corporation
Troy, Michigan

NREL Technical Monitor: Bolko von Roedern

Overview

This report covers the work from September 1 to November 30, 2004 at United Solar Ovonic Corporation under the thin film partnership program supported by NREL. In this quarter, we have worked in the following areas:

1. We have worked on the optimization of Ag/ZnO back reflector for a-SiGe:H and nc-Si:H solar cells. We have improved the deposition process for the Ag and ZnO layers to modify the surface morphology to achieve a high light trapping effect. The newly developed Ag/ZnO back reflector improves not only the short-circuit current density (J_{sc}) by enhancing long wavelength response, but also the fill factor (FF) and the open-circuit voltage (V_{oc}) of a-SiGe:H bottom cells. The improvement in the cell performance correlates to the scattering of light due to improved texture surface.

2. In the area of high rate deposition, we have continued our work on nc-Si:H using MVHF glow discharge. We have explored a new deposition regime under high pressure to enhance the deposition rate. Currently, we are working at ~6-10 Å/s corresponding to an intrinsic layer deposition time of 20-25 minutes. In the last quarterly report, we presented an active-area initial efficiency of 13.8% using an a-Si:H/a-SiGe:H/nc-Si:H triple-junction cell structure made with MVHF at high rates, where the nc-Si:H layer in the bottom cell was deposited for 50 minutes. In this quarter, we did light soaking on some of the high rate triple-junction cells. A stabilized active-area efficiency of 11.3% has been obtained.

3. In the task on large-area deposition, we have continued to optimize the a-SiGe:H middle and bottom cells under the constraints of the production machine. We have also worked on the nc-Si:H solar cells at high deposition rates. Currently, the deposition rate is around 3-5 Å/s, corresponding to an intrinsic layer deposition time of 50-60 minutes. We have achieved an initial aperture-area efficiency of 11.4% using an a-Si:H/nc-Si:H double-junction structure with an aperture area of 45 cm^2.

4. We have continued to study the metastability of nc-Si:H solar cells. We focused on the reverse-bias enhanced light-induced degradation in nc-Si:H solar cells using various experimental methods and proposed a model based on the heterogeneity of the material structure.

1. Optimization of Ag/ZnO back reflector

1.1 Introduction

Solar cell performance depends on many factors including the quality of semiconductor and non-semiconductor layers such as the top and bottom contacts. Especially for thin film solar cells, the semiconductor layers are usually very thin. An optimized top contact not only provides the path for current flow but also reduces the reflection of light. Similarly a textured back contact enhances the absorption of light by trapping the light in the device. In our laboratory, we use Ag/ZnO back reflector (BR) coated stainless steel substrates for high efficiency solar cells. The deposition process for the Ag/ZnO BR was developed for high efficiency a-SiGe:H bottom cells [1]. Due to the difference in material structure between nc-Si:H and a-SiGe:H, an optimum BR for a-SiGe:H cells is not necessarily the best choice for nc-Si:H solar cells. In addition, improving the BR further may also increase the a-SiGe:H cell efficiency. Therefore, we have re-optimized the Ag/ZnO BR in this quarter.

1.2 Experimental

A series of Ag/ZnO BR was deposited using a sputtering system on stainless steel substrates. The texture of the BR was controlled by the deposition parameters such as substrate temperature, pressure, and deposition time. The surface morphology of the BR was characterized using atomic force microscopy (AFM) at NREL. The scattering effect by microstructures on the surface was characterized by measuring the scattering light intensity *versus* the angle between the horizon and the photo-detector as shown in Fig. 1. The light trapping effect was finally evaluated by solar cell performance, especially the long wavelength quantum efficiency (QE) of a-SiGe:H and nc-Si:H solar cells.

Figure 1. Schematic diagram of scattering light intensity measurement setup

1.3 Results and discussion

Figure 2 shows a comparison of AFM images of a conventional and newly optimized Ag/ZnO back reflector. It clearly shows that the average micro-feature size on

Digital Instruments NanoScope
Scan size   4.000 µm
Scan rate   0.7016 Hz
Number of samples   512
Image Data   Height
Data scale   700.0 nm
Engage X Pos
Engage Y Pos

□ view angle
☼ light angle

0 °

X 1.000 µm/div
Z 700.000 nm/div
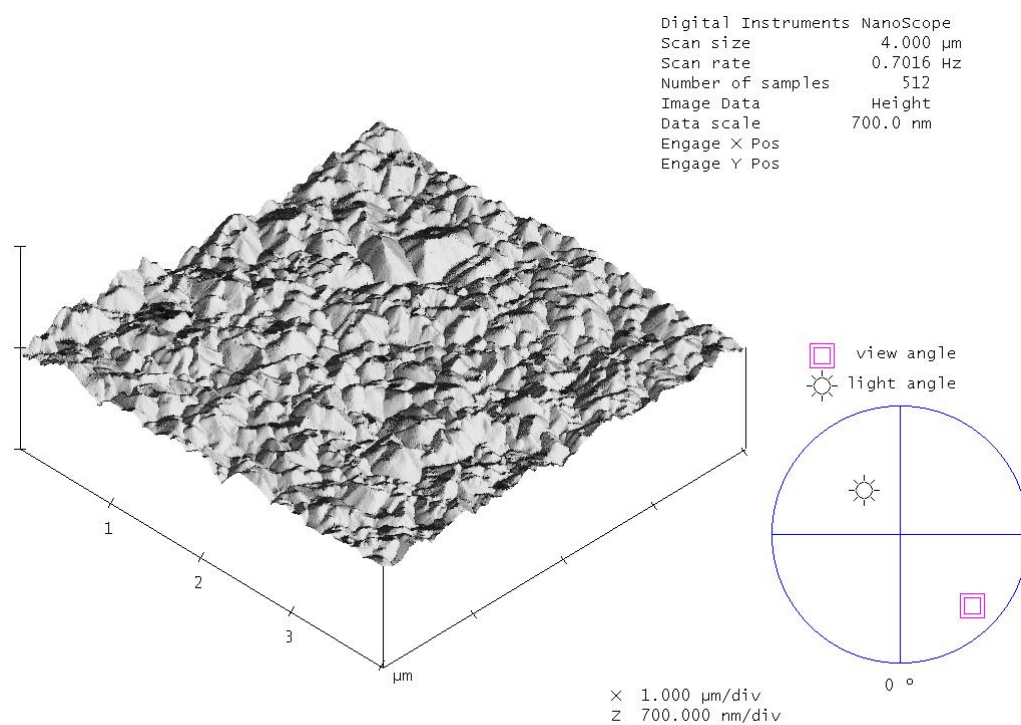
BaoJie Yan, Stainless Steel + back reflector
1748.001

Digital Instruments NanoScope
Scan size   4.000 µm
Scan rate   1.001 Hz
Number of samples   512
Image Data   Height
Data scale   700.0 nm
Engage X Pos
Engage Y Pos

□ view angle
☼ light angle

0 °

X 1.000 µm/div
Z 700.000 nm/div
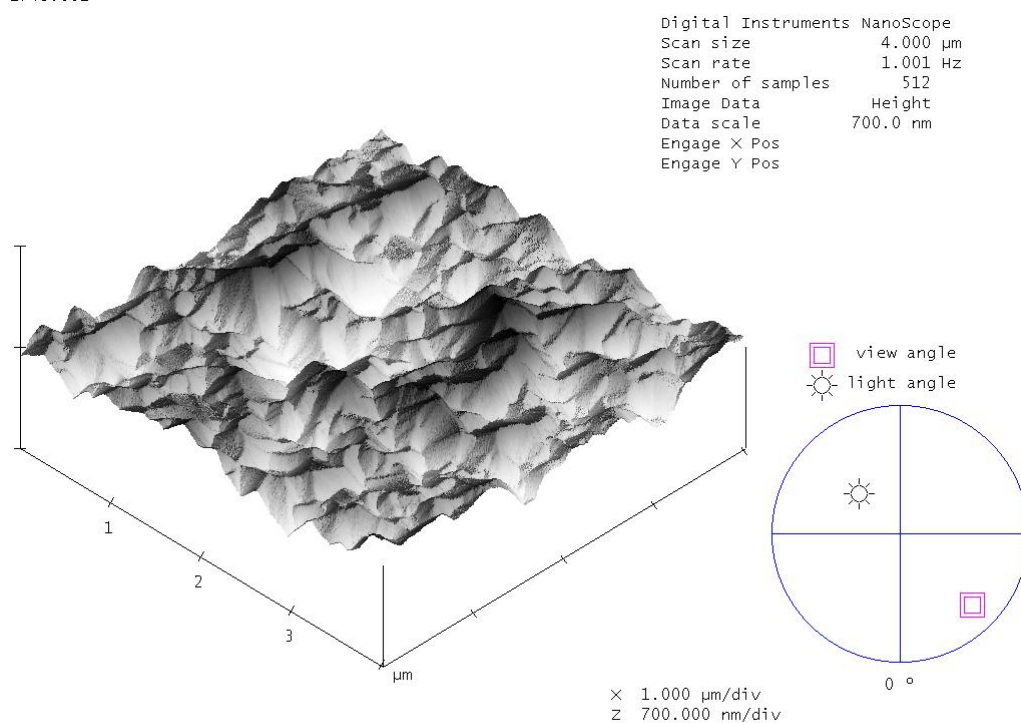
BaoJie Yan, Stainless Steel + back reflector
7631.001

Figure 2. AFM pictures of a conventional (upper) and a newly optimized (lower) Ag/ZnO back reflectors.

4

Table I: J-V characteristics of a-SiGe:H middle and bottom cells made on stainless steel (SS), conventional Ag/ZnO back reflector, and improved Ag/ZnO back reflector.

Cell Type	Sample No.	J_{sc} (mA/cm^2)	V_{oc} (V)	FF	E_{ff} (%)	Substrate
a-SiGe middle cell	15112	15.42	0.779	0.662	7.95	SS
	15052	20.46	0.758	0.557	8.64	Standard BR
	15051	20.99	0.769	0.634	10.23	Improved BR
a-SiGe bottom cell	15064	15.98	0.669	0.628	6.71	SS
	15065	22.99	0.666	0.594	9.09	Standard BR
	15066	23.78	0.69	0.61	10.01	Improved BR

the new BR is much larger than that on the conventional one. Figure 3 plots the scattered light intensity *versus* the angle θ as illustrated in Fig. 1 for the two BRs. It clearly shows that the new BR scatters light more efficiently than the conventional one. Since the scattered light is measured at a wavelength of 632.8 nm and does not give a complete picture under the solar spectrum, the final qualification has to be measured by solar cell performance. Figure 4 shows a comparison of quantum efficiency (QE) for solar cells deposited on conventional and improved Ag/ZnO back reflectors, where the upper plot is for nc-Si:H cells and the lower plot for a-SiGe:H bottom cells. It shows that the cell deposited on the improved back reflector has an enhanced long wavelength response without the interference fringes. The total J_{sc} increases by 1.0 to 1.5 mA/cm^2.

Another interesting phenomenon is that the new BR improves not only the J_{sc} but also the open-circuit voltage (V_{oc}) and fill factor (FF) for a-SiGe:H middle and bottom cells as shown in Table I. Compared to the cells deposited on stainless steel (SS) substrate, solar cells made with the same recipe but on textured Ag/ZnO back reflector substrate normally show a higher J_{sc} due to the light trapping effect, but a lower V_{oc} due to the high dark current density, and a lower FF due to wider Fermi level splitting and higher effective series resistance. This phenomenon is clearly shown by the comparison of the solar cells on SS and on the conventional back reflectors as shown in Table I. However, the losses in V_{oc} and FF due to the textured back reflector are reduced for the cells on the new back reflector. Especially for the a-SiGe:H bottom cell, the V_{oc} of the cell on the improved back reflector is even higher than that on SS. Such improvement in V_{oc} and FF has not been found in a-Si:H and nc-Si:H single-junction solar cells. To understand why the new back reflector improves the V_{oc} and FF, one needs to understand the mechanism of losing V_{oc} and FF when solar cells are deposited on textured back reflector. As mentioned above, the high dark current could be the reason for lower V_{oc} in the cell on textured back reflector than that on specular SS substrate. The high dark current density could result from the enhanced effective area as previously understood. It could also result from the sharp peaks on the back reflector surface as shown in Fig. 2. First, there may be strong possibility for carriers to diffuse back into the doped layers at the peaks. Second, there might be a high probability to form filaments at the peak positions. Comparing the AFM pictures in Fig. 2, the peak density in the newly improved back reflector has been significantly reduced with an increased microfeature size. With the enlarged microfeatures, the light trapping effect has been improved for high
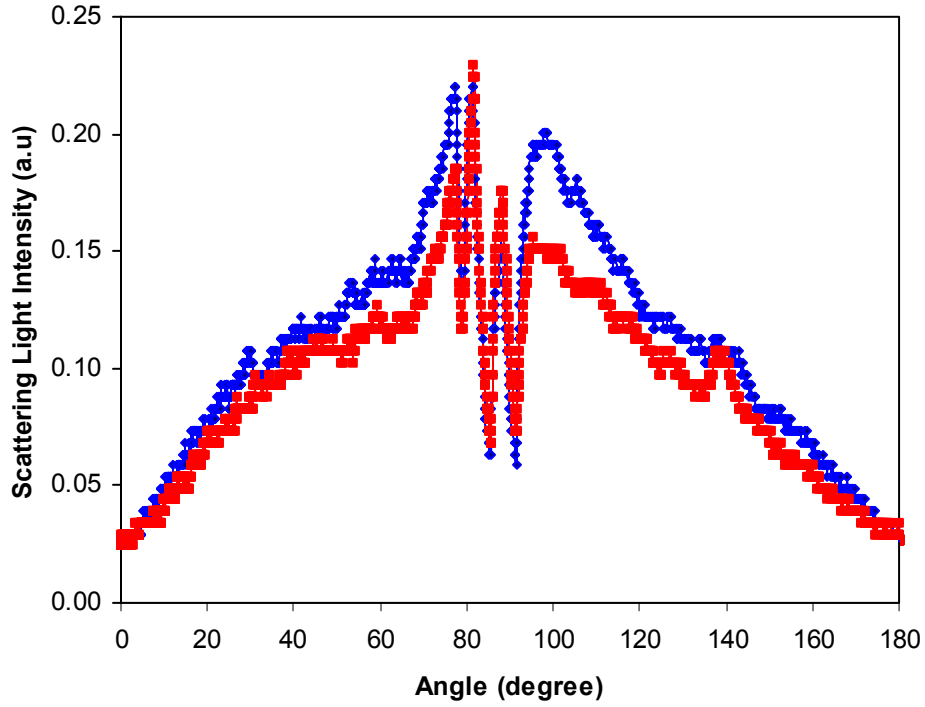
Figure 3. Scattering light intensity versus the angle as shown in Fig. 1 for a conventional Ag/ZnO BR (red) and a newly re-optimized one (blue).

current density and, at the same time, the reduced peak density on the surface improves V_{oc} and FF for a-SiGe:H solar cells.

1.4 <u>Summary</u>

We have optimized the Ag/ZnO back reflector for both nc-Si:H and a-SiGe:H solar cells. A gain of 1-1.5 mA/cm^2 in J_{sc} has been obtained in both nc-Si:H and a-SiGe:H solar cells. In addition, an improvement in V_{oc} and FF is also observed for a-SiGe:H cells deposited on the new back reflector. We propose a possible mechanism for the improvement.
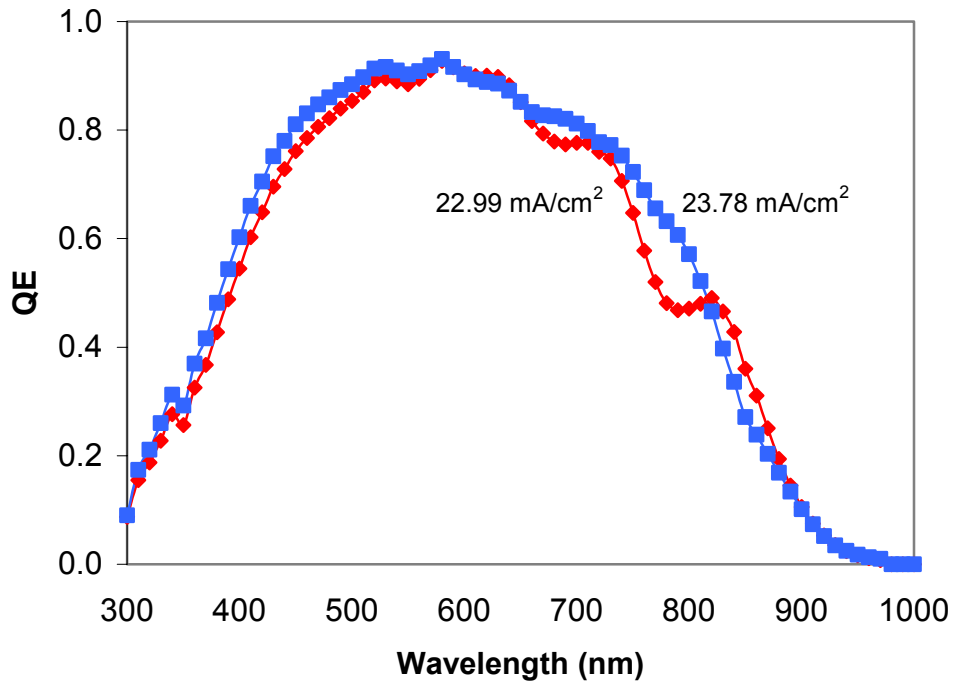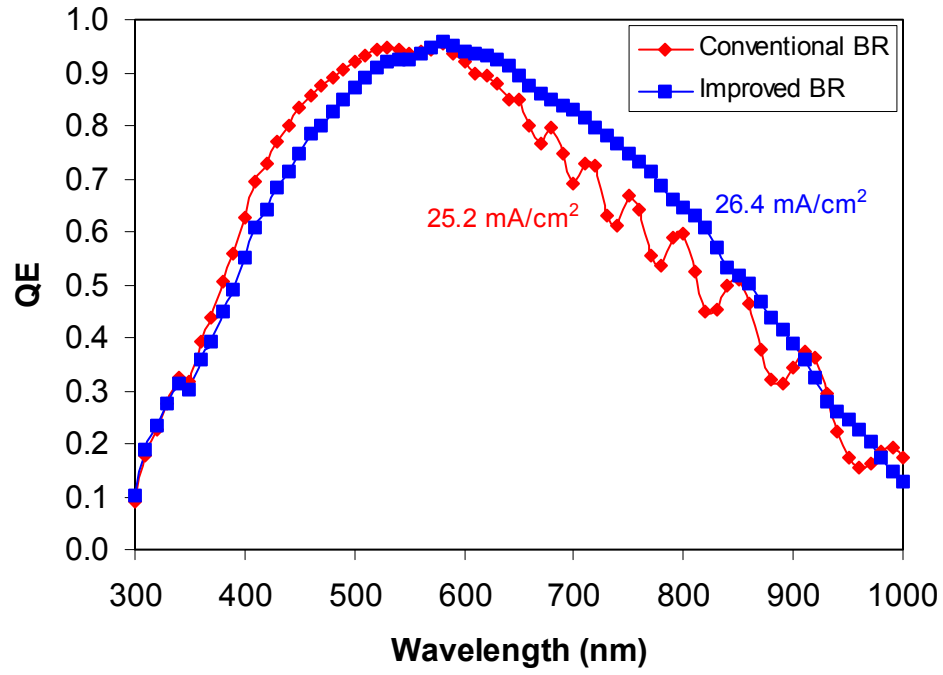
Figure 4. Quantum efficiency of nc-Si:H (upper) and a-SiGe:H (lower) solar cells deposited on conventional (red) and newly optimized (blue) Ag/ZnO back reflector substrates.

2. a-Si:H/a-SiGe:H/nc-Si:H triple-junction solar cells made by MVHF

In order to prevent the microstructure evolution in nc-Si:H material, a hydrogen dilution profiling technique has been developed [2], where the hydrogen dilution ratio was decreased during deposition. This technique has been proven successful in improving the cell efficiency in both RF at low rate and VHF at high rate depositions. In the last quarter, we reported an initial active-area efficiency of 13.8% in an a-Si:H/a-SiGe:H/nc-Si:H triple-junction solar cell, where the nc-Si:H bottom cell was made by MVHF glow discharge using the hydrogen dilution profiling technique. In this quarter, we finished the stability experiment on the high efficiency a-Si:H/a-SiGe:H/nc-Si:H triple-junction solar cells. The standard light soaking condition has been used with 100 mW/cm^2 of white light at 50 ºC for 1000 hours.

Table II lists initial and stable J-V characteristics of a series of a-Si:H/a-SiGe:H/nc-Si:H triple-junction solar cells. The stable efficiency of the champion cell is 11.3%, which showed 18% degradation. The relatively large degradation is likely caused by the combination of the larger degradation in the thicker a-Si:H top cell and a-SiGe:H middle cell, and nearly matched current densities between the component cells. We have also tried to reduce the deposition time of the nc-Si:H intrinsic layer in the bottom cell. The deposition time of the bottom cell intrinsic layer in the cell RF12876 is 50 minutes, which is 10 minutes shorter than that for cell RF12852. The stable efficiency for this cell is also 11.3%.

Table II: Stability results of three a-Si:H/a-SiGe:H/nc-Si:H triple junction solar cells, where the nc-Si:H bottom cell was made using MVHF at high rates.

Sample No.	Status	Q (mA/cm^2)				V_{oc} (V)	FF	P_{max} (mW/cm^2)	Comments
		Top	Mid	Bott	Total				
12852	Initial	8.21	8.17	8.08	24.46	2.175	0.786	13.8	60 min bottom cell
	Stable	8.00	7.76	7.91	23.67	2.095	0.692	11.3	
	Deg.	2.56%	5.02%	2.10%	3.23%	3.85%	8.34%	18.0%	
12863	Initial	8.54	8.04	8.39	24.97	2.163	0.744	12.9	60 min bottom cell
	Stable	8.27	7.70	8.41	24.38	2.086	0.656	10.5	
	Deg.	3.16%	4.23%	0	2.36%	3.52%	9.02%	18.6%	
12876	Initial	8.31	8.15	8.25	24.71	2.195	0.737	13.2	50 min bottom cell
	Stable	7.97	7.90	8.18	24.05	2.110	0.676	11.3	
	Deg.	4.09%	3.07%	0.85%	2.67%	3.52%	5.45%	14.4%	

3. Large-area deposition of nc-Si:H solar cells at high deposition rate

We have reported an initial efficiency of 11.3% using an a-Si:H/nc-Si:H double-junction cell deposited with RF at low rate on a large area substrate with an aperture area of 460 cm^2 [3]. After encapsulation and light soaking, this cell showed an efficiency of 9.4% measured at United Solar and 9.2% measured at NREL. In this quarter, we have investigated the effect of increasing the deposition rate by increasing the pressure and RF power and studied the performance of nc-Si:H solar cells on Ag/ZnO back reflector where the nanocrystalline layer was deposited in 50 minutes using the large area deposition system (2B). It has been reported that when using higher power density to increase the growth rate of nanocrystalline material, higher deposition pressure reduces ion bombardment energy thus increasing the grain size [4], and leads to higher solar cell efficiency as well as stability to atmospheric oxidation [5]. Table III shows the typical performance characteristics as a function of deposition pressure.

Table III: nc-Si:H solar cell performance for several runs at different deposition pressures. The cells have an active area of 0.25 cm^2.

Cell #	V_{oc} (V)	FF	Pressure	J_{sc} (mA/cm^2)	Efficiency (%)
10138 LC1	0.336	0.407	Low	18.02	2.46
10153 LC1	0.460	0.644	Medium	20.90	6.19
10192 LC1	0.484	0.666	High	22.62	7.29

We observe that the performance improves as the pressure increases. This can be attributed to two factors [4] – (i) the ion bombardment decreases and allows the growth of larger crystallites and (ii) the ratio of flux of hydrogen atoms to silyl (SiH$_3$) radicals at the growth surface decreases due to a combination of lower electron temperature and reduced mean free path. The net effect of these factors is to move the deposition regime towards lower dilution and the amorphous – nanocrystalline phase boundary. The highest AM1.5 efficiency is not necessarily suitable for use as the bottom cell. We evaluate the latter from J_{sc} using a 610-nm long pass filter. The results for the best cell in Table IV are compared with others where the AM1.5 efficiencies are lower but the red light J_{sc} is higher.

Table IV: nc-Si:H solar cell parameters under AM 1.5 and >610nm filtered illumination for several deposition runs.

Cell #	Area (cm^{-2})	Spectrum	V_{oc} (V)	FF	J_{sc} (mA/cm^2)	P_w (mW/cm^2)
10192 LC1	0.25	AM1.5	0.484	0.666	22.62	7.29
10192 LC1	*0.25*	*>610*	*0.462*	*0.684*	*11.19*	*3.61*
10228 LC1	0.25	AM1.5	0.456	0.496	23.09	5.22
10228 LC1	*0.25*	*>610*	*0.433*	*0.579*	*11.98*	*3.00*
10287 LC1	0.25	AM1.5	0.46	0.534	23.06	5.66
10287 LC1	*0.25*	*>610*	*0.437*	*0.599*	*11.95*	*3.13*

Another factor to be taken into consideration is the uniformity. We find that the uniformity of the performance is poor when we use the highest pressure. In fact, some of the edge areas are amorphous. Therefore, to obtain uniform performance over large areas we opted to optimize the pressure and hydrogen dilution combination. The comparison for center (LC1)

and edge (N) samples is shown in Table V. We see from the V_{oc} values in Table V, that the conditions contributing to the highest efficiency nc-Si:H in the central region result in the cells at the edges show amorphous signature similar to our previous report [6]. On the other hand, the adjustment of pressure and dilution allows fabrication of much more uniform cells.

Table V: nc-Si:H solar cell parameters from the central (LC1) and edge (N) regions for several deposition runs. An active-area of 0.25 cm^2 is defined on top of the *p* layer by the ITO dots and the grids.

Cell #	V_{oc} (V)	FF	J_{sc} (mA/cm^2)	P_w (mW/cm^2)
10192 LC1	0.484	0.666	22.62	7.29
10192 N	*0.991*	*0.625*	*17.06*	*10.57*
10228 LC1	0.456	0.496	23.09	5.22
10228 N	*0.498*	*0.518*	*22.75*	*5.87*
10304 LC1	0.448	0.569	22.78	5.81
10304 N	*0.487*	*0.58*	*22.98*	*6.49*

We have investigated the degradation behavior of several nc-Si:H silicon cells. We selected cells having a variety of open circuit voltage values. The cells were light soaked under 100 mW/cm^2 of white light for about 330 hours at 50 °C. Subsequently, they were annealed at 150 °C in vacuum for 2 hours. Figure 5 shows the variation of the V_{oc} of these cells. The V_{oc} degrades to different extents and recovers on annealing. The corresponding FF variations are shown in Fig. 6. Some of the FFs degrade but do not appear to recover.
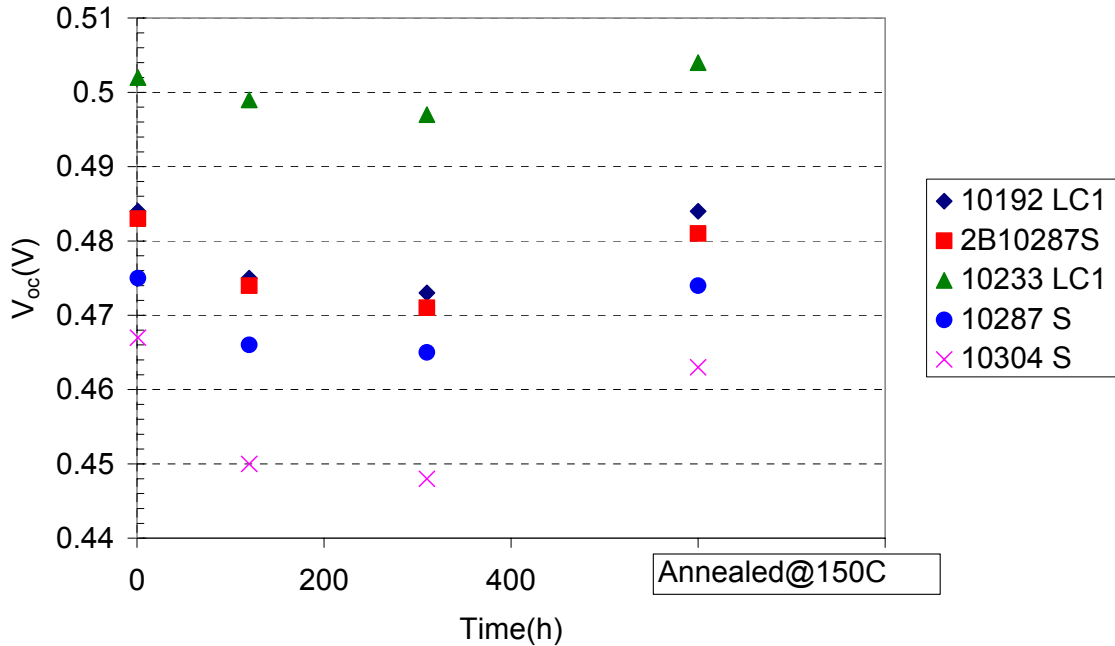

Figure 5. The initial, light soaked, and annealed open circuit voltage of nanocrystalline cells having a range of initial open circuit voltages.
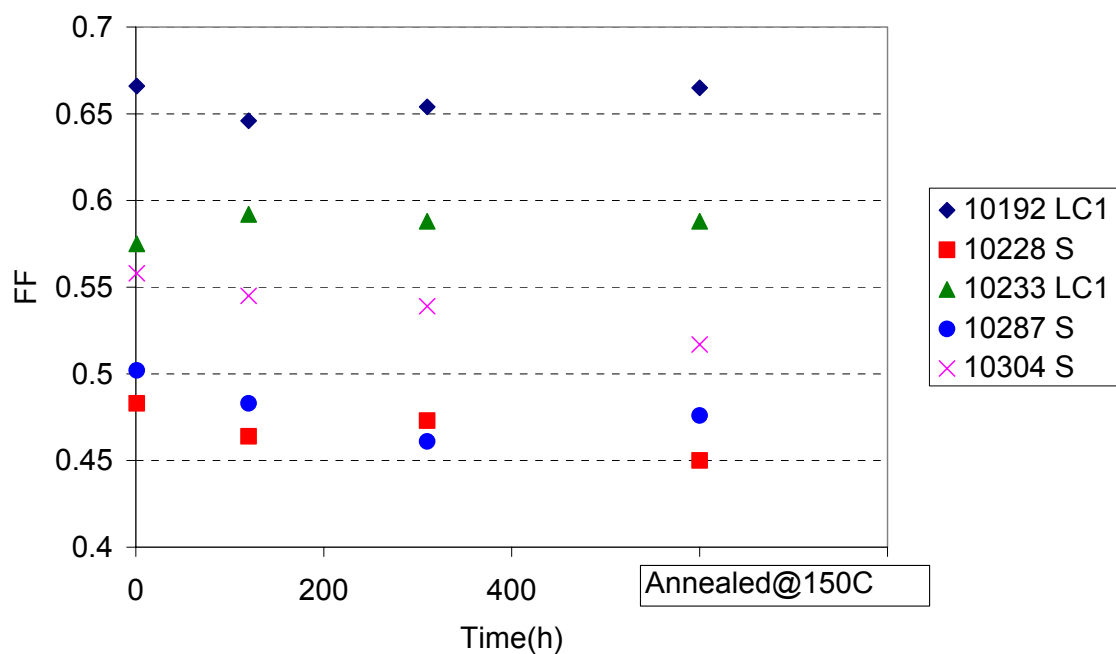
Figure 6. The initial, light soaked, and annealed fill factors of nanocrystalline cells having a range of initial open circuit voltages.
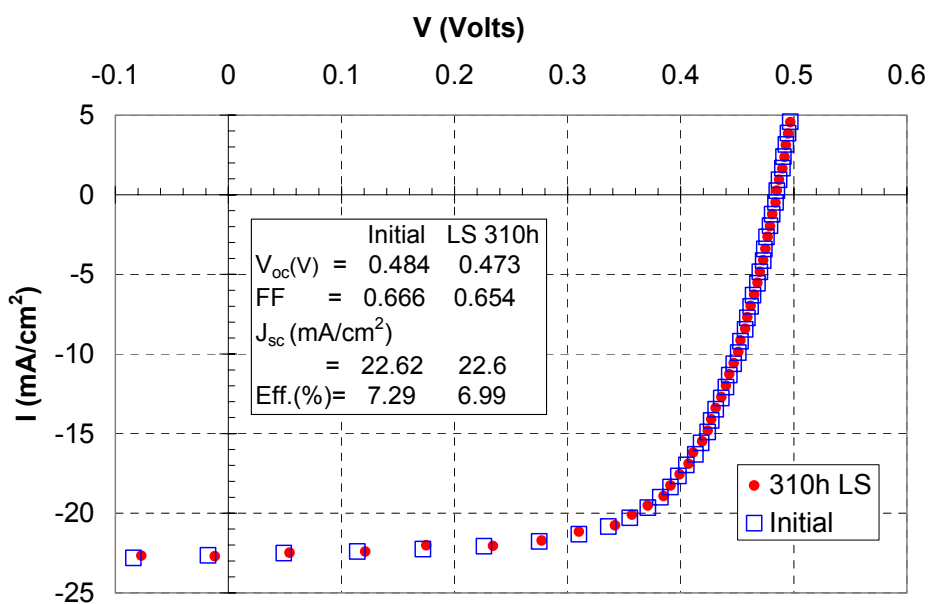
Figure 7. The J-V characteristics of sample # 10192LC1 in the initial state, and after light soaking for 310 hours under 100 mW/cm^2 of white light illumination at ~50°C.

The J-V curves for sample 10192LC1 in the initial state, and after light soaking for 310 hours are shown in Fig. 7. The initial performance is about 7.3% and it degrades by about 4% to about 7.0%. The loss is equally divided between the FF (2%) and Voc (2%). The cell

11

parameters for all 5 cells are tabulated in Table VI. We note that the overall degradation varies between 0 and 10%. The degradation of the FF varies between 2 - 8% while that of V_{oc} varies between 1 – 4%. The current does not change within the measurement uncertainty.

Table VI: The parameters of several nc-Si cells having different V_{oc} in the initial and 310h light soaked state.

| Cell #	Area (cm^2)	State	Voc (V)	FF	J_{sc} (mA/cm^2)	Efficiency (%)
10192 LC1	0.25	Initial	0.484	0.666	22.62	7.29
		LS 310h	0.473	0.654	22.6	6.99
		Degr.	*2.27%*	*1.8%*	*0.1%*	*4.1%*
10228 S	0.25	Initial	0.483	0.483	22.75	5.31
		LS 310h	0.471	0.473	22.88	5.10
		Degr.	*2.48%*	*2.07%*	*-0.57%*	*3.96%*
10233 LC1	0.25	Initial	0.501	0.575	21.1	6.08
		LS 310h	0.497	0.588	21.04	6.15
		Degr.	*0.80%*	*-2.26%*	*0.28%*	*-1.16%*
10286 S	0.25	Initial	0.475	0.502	22.98	5.48
		LS 310h	0.465	0.461	23.09	4.95
		Degr.	*2.11%*	*8.17%*	*-0.48%*	*9.67%*
10304 S	0.25	Initial	0.467	0.558	22.87	5.96
		LS 310h	0.448	0.539	22.7	5.48
		Degr.	*4.07%*	*3.41%*	*0.74%*	*8.02%*
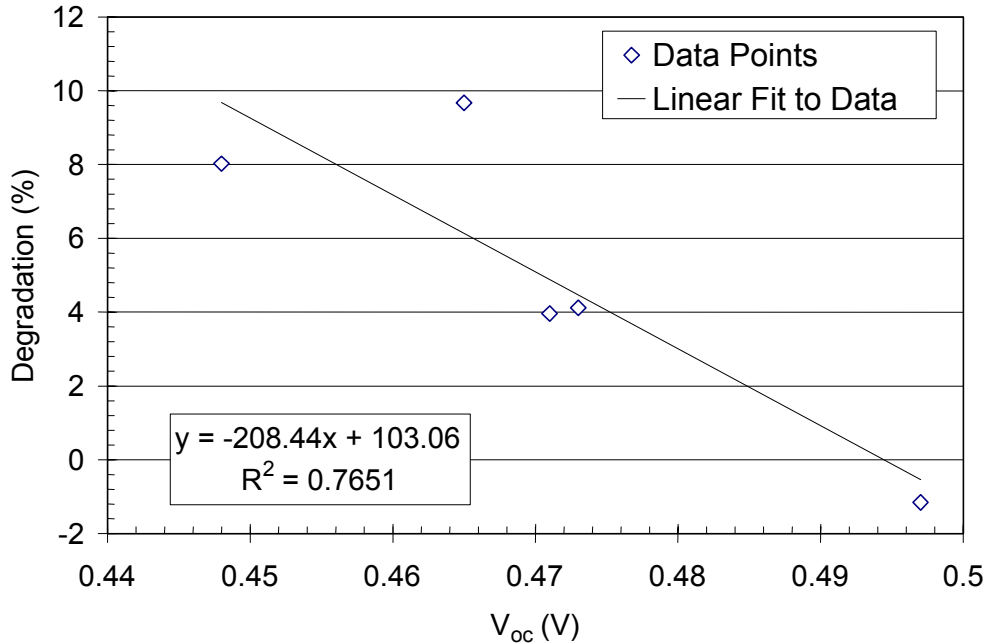
Figure 8. The overall degradation of 5 different nanocrystalline silicon cells as a function of their open circuit voltage.

Fig. 8 shows the correlation between V_{oc} and the overall degradation after light soaking. Surprisingly, this limited data set shows the degradation decreasing with increasing V_{oc} within the nanocrystalline silicon deposition parameter space covered. The V_{oc} in nc-Si:H cells has previously been correlated with the crystalline fraction from Raman scattering [7] as well as X-ray diffraction data [8]. Considering that the degradation is expected to occur in the amorphous regions [9], one would have expected the reverse trend in Fig. 8. It would be interesting to expand the data set to verify a more general trend.

We have also optimized the performance of a-Si:H/nc-Si:H tandem cells with both low rate and higher rate deposited a-Si:H top cells combined with higher rate deposited nc-Si bottom cells. We see in Table VII that both types of tandem cells can be obtained with >11% efficiency. The best stabilized efficiency obtained after over 300 hours of light soaking is 10.4%. The tandem cells with lower rate deposited top cells degrade 7- 9% while those with high rate deposited top cells degrade 14-17%.

Table VII: J-V characteristics of a-Si:H/nc-Si:H double-junction solar cells with an active area of 0.25 cm^2 in the initial and light soaked state.

Run #	Cell #	State	V_{oc}	FF	J_{sc} QE Top	J_{sc} QE Bot	Eff	Comments
			(V)		(mA/cm^2)		(%)	
10241 LC1	33	Initial	1.422	0.727	10.82	11.49	11.19	Low Rate Top Cell
		LS 330h	1.385	0.69	10.84	11.66	**10.36**	
		Degr.	*2.60*	*5.09*	*-0.18*	*-1.48*	*7.39*	
10241 N	32	Initial	1.430	0.720	10.75	11.75	11.05	Low Rate Top Cell
		LS 330h	1.399	0.676	10.6	11.75	10.02	
		Degr.(%)	*2.24*	*5.85*	*1.40*	*0*	*9.24*	
10241 S	32	Initial	1.437	0.734	10.73	11.49	11.32	Low Rate Top Cell
		LS 330h	1.400	0.686	10.54	11.46	10.29	
		Degr.(%)	*2.20*	*5.31*	*1.77*	*0*	*8.94*	
10365 LC1	23	Initial	1.415	0.748	11.53	10.92	11.56	High Rate Top Cell
		LS 330h	1.376	0.648	10.64	10.7	9.49	
		Degr.(%)	*2.76*	*13.4*	*7.70*	*2.00*	*16.9*	
10365 N	33	Initial	1.448	0.733	11.52	10.58	11.23	High Rate Top Cell
		LS 330h	1.416	0.657	10.53	10.34	9.62	
		Degr.(%)	*2.20*	*10.4*	*8.59*	*2.27*	*14.3*	

Table VIII: Initial J-V characteristics of a-Si:H/nc-Si:H double-junction solar cells with an aperture area of 45.5 cm^2.

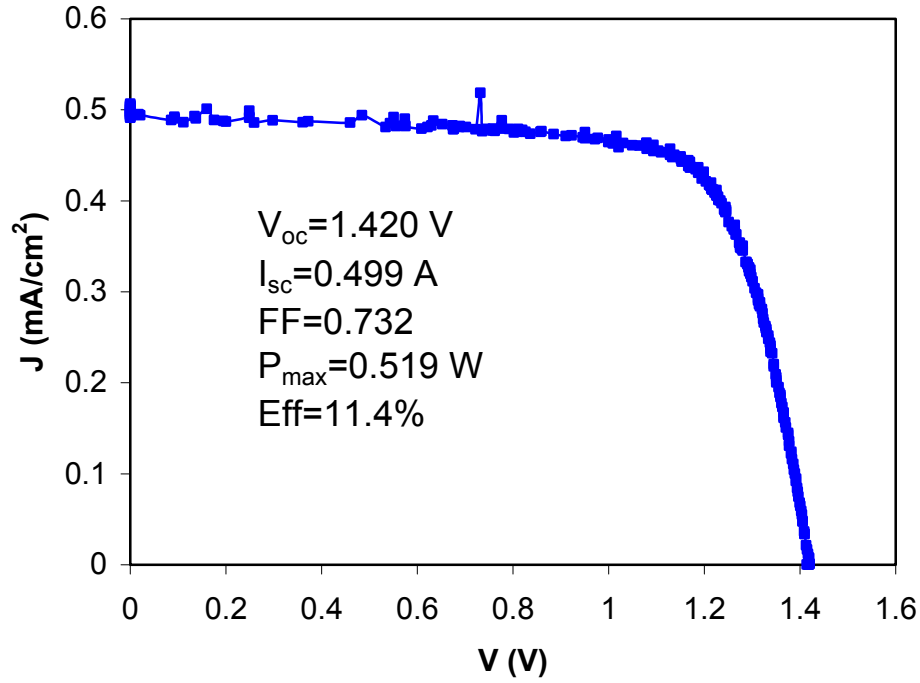| Run #	V_{oc} (V)	I_{sc} (A)	FF	P_{max} (W)	Eff (%)
10389F2	1.428	0.489	0.736	0.514	11.30
10389G2	1.425	0.492	0.729	0.512	11.25
10389G3	1.436	0.489	0.715	0.502	11.04
10390E1	1.419	0.492	0.728	0.508	11.17
10390E2	1.415	0.483	0.752	0.514	11.29
10390E3	1.431	0.486	0.722	0.502	11.03
10390F1	1.424	0.502	0.720	0.514	11.30
10390F2	1.420	0.499	0.732	0.519	**11.40**
10390G1	1.424	0.498	0.721	0.512	11.25
10390G2	1.422	0.573	0.615	0.501	11.01

Figure 9. Initial J-V characteristics of an a-Si:H/nc-Si:H double-junction solar cell with an aperture area of 45 cm^2. The intrinsic nc-Si:H layer in the bottom cell used a deposition time of 50 minutes.

We have also made a-Si:H/nc-Si:H double-junction cells using the high rate nc-Si:H bottom cell with an aperture area of 45 cm^2. Table VIII lists the initial performance of some cells. The highest initial efficiency is 11.4%. Figure 9 shows the J-V characteristics of the best cell. These cells are under light soaking and the stable efficiency will be presented in the future. Currently we are in the process of using these optimized conditions to fabricate a-Si:H/nc-Si:H double-junction modules with an aperture area of 460 cm^2 using the 50-minute deposition time for the nc-Si:H bottom cell.

In summary, we optimized nc-Si:H single-junction and a-Si:H/nc-Si:H double-junction solar cells using RF glow discharge in a large-area machine at high deposition rate. High quality nanocrystalline cells have been fabricated at higher deposition rates by increased the pressure and RF power. An initial active-area (0.25 cm^2) efficiency of 7.3% has been achieved with 50 minutes nc-Si:H intrinsic layer deposition time. This cell stabilized at 7.0% after light soaking at 50 °C. We optimized 0.25cm^2 a-Si:H/nc-Si:H double-junction cells and obtained an initial, active area efficiency of 11.6%. The highest, stabilized efficiency was 10.4% after light soaking at 50°C. We have also made cells with an aperture area of 45 cm^2 and achieved an initial cell efficiency of 11.4%.

14

4. Effect of electrical bias on metastability in hydrogenated nanocrystalline silicon solar cells

4.1 Introduction

In the last quarterly report, we presented a surprising observation of reverse bias enhanced light-induced degradation in nc-Si:H solar cells, which is contrary to the case in a-Si:H solar cells. For a-Si:H solar cells, light-induced degradation is suppressed by a reverse bias due to the enhanced electric field in the intrinsic layer, where photo-generated electron and hole pairs are separated by the electric field. The reverse bias enhanced light-induced degradation is very puzzling. We have initially proposed a back-to-back diode model based on the heterogeneity of the material structure. In this quarter, we have continued to study the bias dependence of the light-induced degradation of nc-Si:H solar cells. Four experiments have been carried out. We first present the dependence of light-induced degradation in nc-Si:H solar cells on the magnitude of external bias. We measured the cell performance under standard condition of AM1.5 illumination at 25 °C as well as under red and blue lights with low intensities. Second, we show the results of quantum efficiency loss for the nc-Si:H cells after the degradations under various bias conditions. Third, we show the results of light-induced degradations under reverse bias with different light spectra. Finally, we show light-assisted annealing of defects generated by light soaking under reverse bias. We find that the light-induced degradation under reverse bias can partially recover during light soaking under open-circuit condition. Based on the experimental observations, we present a detailed explanation based on our previous back-to-back diode model [9].

4.2 Experimental

Similar to the previous report, single-junction, 1 μm thick nc-Si:H and 0.2 μm thick a-Si:H *nip* solar cells were deposited on 4 cm × 4 cm Ag/ZnO back reflector (BR) coated stainless steel (SS) substrates and specular SS substrates, respectively. The intrinsic layers were deposited using a modified very high frequency glow discharge with a SiH_4 and H_2 mixture at high deposition rates of 3-8 Å/s. The solar cells were completed with indium-tin-oxide dots having an active-area of 0.25 cm^2 on the top *p* layer. Current densities versus voltages, *J-V*, characteristics were measured under an AM1.5 solar simulator at 25 °C. Quantum efficiency (QE) measurements were made at room temperature under short circuit condition and also under a reverse bias of 1 V when needed. Quantum efficiency loss (Q_{loss}) was calculated by the ratio of QE under –1 V to QE under short-circuit condition. Light soaking experiments were carried out using 100 mW/cm^2 of white light at 25 °C and 50 °C under open-circuit condition or under an electrical bias. Light soaking was also carried out with different light spectra under a reverse bias of 1 V. The red light was obtained by using the white light source with a 665 nm cut-on filter, and the blue light with a 650 nm cut-off filter. The light intensities for different spectra were adjusted to have the same J_{sc} for a given solar cell. For most experiments, both a-Si:H and nc-Si:H cells were included for comparison. The samples were annealed in vacuum at 150 °C for 2 hours before and after light soaking or current injection.

4.3 <u>Results</u>

4.3.1 Bias dependence of light-induced degradation in nc-Si:H solar cell

  A reverse electrical bias causes significant enhancement of the light-induced degradation in the nc-Si:H solar cells [9]. Therefore, it is very interesting to investigate the dependence of degradation on the magnitude of the applied bias. We selected solar cells from the same substrate with very good uniformity of the cell performance and light-soaked the cells simultaneously under 100 mW/cm^2 of white light at 50 ^{o}C under various bias conditions of –1 V, short circuit, open circuit, and +1 V. To check the reproducibility of the degradation rate, we included two cells at each bias condition. Table IX summarizes the J-V characteristics of the initial state and degraded state reached after 309 hours of light soaking. The values of FF under blue and red light illumination, FF_b and FF_r, were measured using narrow band-pass filters centered at 390 nm and 670 nm, respectively, at low light intensities. One can see that the cells with the same bias condition have similar degradation rates. The light-induced degradation of the FF under AM1.5 illumination as a function of the applied bias is plotted in Fig. 10 (a), where the short circuit condition corresponds to 0 V bias, and the open circuit is considered to be a forward bias with a bias value of V_{oc}, which is around 0.48 V. It clearly shows that the light-induced degradation increased with the increase of the magnitude of reverse bias. The FF degraded on average by 10.9% under the reverse bias condition of 1 V, 7.6% under short circuit condition, 3.8% under open circuit condition, and 3.8% under 1 V of forward bias.

  Figure 10 (b) shows the degradation in FF_b and FF_r as well as their ratio as a function of the applied bias. Normally, for a uniform one-phase material, FF_b is a measure of the properties near the *i/p* interface since the blue light is mainly absorbed in this region. Moreover, since the holes have a very short distance to traverse under blue light illumination, FF_b is also determined by electron transport. FF_r is a measure of hole transport in the bulk of the material since the red light is more uniformly absorbed. However, in nc-Si:H solar cells, the FF_b and FF_r are not only affected by the properties of the material in different regions of the intrinsic layer, but also by the heterogeneity of the material in the intrinsic layer. This is because higher energy photons (blue light) are mainly absorbed in the amorphous phase while the lower energy photons (red light) in the crystalline phase. One notes that the bias dependence of FF_r degradation is similar to that of FF degradation measured under AM1.5 illumination as shown in Fig. 10 (a). However, under the reverse bias and short circuit conditions, the FF_r has more degradation than the FF_b whereas the FF_b has more degradation under the forward bias. The change of the ratio of FF_b to FF_r has a monotonic increase as the applied bias increases from negative to positive.

Table IX. J-V characteristics of the initial (In.) and degraded (Deg.) nc-Si:H solar cells. The light soaking was done under one sun white light with various bias conditions of –1 V, short circuit, open circuit, and +1 V at 50 $^{\circ}$C.

| Cell No.	Bias (V)	Status	V_{oc} (V)	ΔV_{oc} (mV)	FF	ΔFF /FF_{in} (%)	FF_b	ΔFF_b /FF_{bin} (%)	FF_r	ΔFF_r /FF_{rin} (%)
1	-1 V	In.	0.479		0.634		0.663		0.664	
		Deg.	0.464	-15	0.563	-11.2	0.624	-5.9	0.579	-12.8
2		In.	0.479		0.633		0.659		0.664	
		Deg.	0.464	-15	0.566	-10.6	0.624	-5.3	0.580	-12.7
3	Short circuit	In.	0.483		0.618		0.664		0.660	
		Deg.	0.472	-9	0.580	-6.1	0.636	-4.2	0.617	-6.5
4		In.	0.480		0.631		0.663		0.663	
		Deg.	0.474	-6	0.574	-9.0	0.638	-3.8	0.599	-9.7
5	Open circuit	In.	0.477		0.622		0.650		0.653	
		Deg.	0.470	-7	0.600	-3.5	0.617	-5.1	0.622	-4.7
6		In.	0.478		0.628		0.655		0.655	
		Deg.	0.470	-8	0.603	-4.0	0.618	-5.6	0.622	-5.0
7	+1 V	In.	0.482		0.608		0.655		0.655	
		Deg.	0.467	-15	0.587	-3.5	0.607	-7.3	0.621	-5.2
8		In.	0.478		0.629		0.656		0.651	
		Deg.	0.465	-13	0.604	-4.0	0.612	-6.7	0.624	-4.1
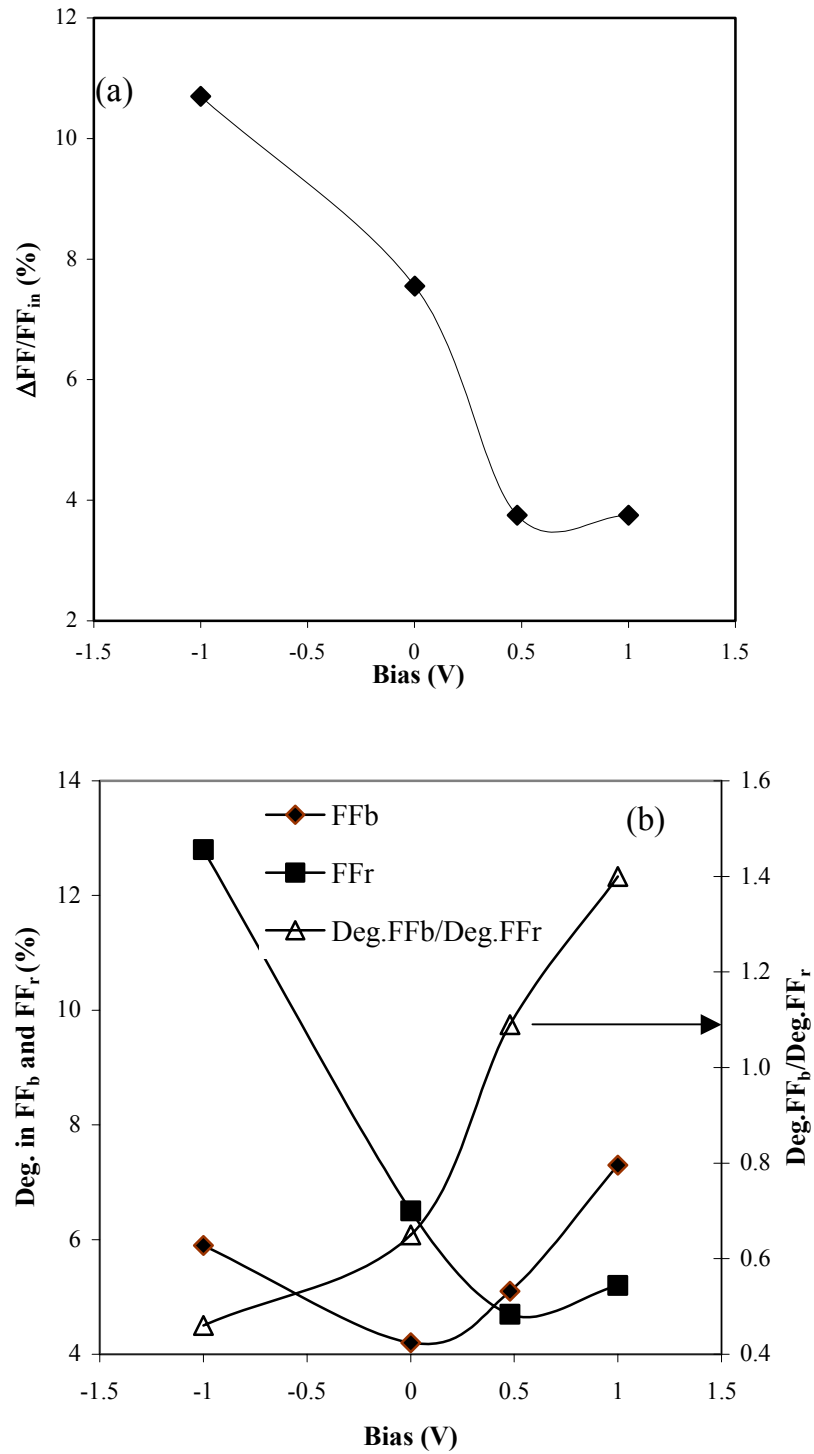
Figure 10. (a) Light-induced degradation in FF and (b) FF_b, FF_r of nc-Si:H solar cells versus the electrical bias during light soaking, where ΔFF denotes the variations in FF. Light soaking was carried out at 50 ^{o}C under one sun white light for 309 hours

4.3.2 Light-induced quantum loss of nc-Si:H solar cell

Banerjee *et al.* [10] used a quantum efficiency loss technique to study a-Si:H and a-SiGe:H alloy cells with different intrinsic layers and *p/i* interfaces, and identified the carrier collection losses at the *p/i* interface and the bulk of the *i* layers. We used the same technique to investigate light-induced degradation of nc-Si:H cells. The quantum efficiencies of the solar cells under short circuit condition, ($Q(0\ V)$), and under reverse bias of 1 V ($Q(-1\ V)$) were measured and the quantum efficiency loss, Q_{loss}, was defined as the ratio of $Q(-1\ V)$ to $Q(0\ V)$. Usually, the Q_{loss} values at 390 and 670 nm have correlations with the values of FF_b and FF_r, respectively. High values of FF_b and FF_r are associated with low values of Q_{loss} at 390 and 670 nm, and *vice versa*. Figure 11 shows the Q_{loss} as a function of the wavelength for two cells. One cell was light-soaked under a reverse bias condition, and the other under open circuit condition. For their initial states, the Q_{loss} spectra are the same, indicating that the two cells have a similar carrier collection. After light soaking, the two Q_{loss} curves became significantly different. The cell under the reverse bias condition shows much higher Q_{loss} than the cell under open circuit condition in the long wavelength region, and lower Q_{loss} in the short wavelength region. The result is consistent with the FF_b and FF_r measurements shown in Fig. 10(b).
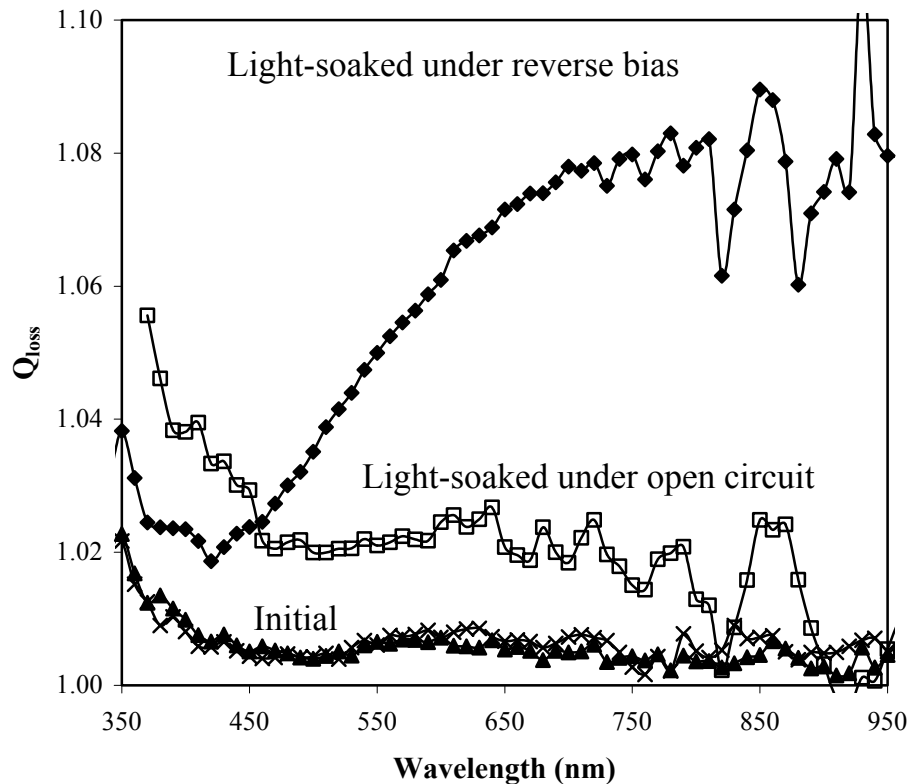

Figure 11. Q_{loss} spectra of nc-Si:H cells before and after light soaking with and without reverse bias. Q_{loss} is defined as the ratio of the biased to the short circuit quantum efficiency.

19

4.3.3 Light-induced degradation with different light spectra under reverse bias

As mentioned above, we have carried out the light-soaking experiment on nc-Si:H solar cells with different light spectra under open circuit condition [11]. We found that illumination on nc-Si:H solar cells using a red light with photon energies lower than the bandgap of a-Si:H did not result in any degradation in the cell performance, whereas both blue and white light illumination cause degradation, with the blue light degradation slightly larger than that due to white light. Since the red light is only weakly absorbed in the amorphous phase, but is readily absorbed in the nanocrystalline grains, we concluded that the light-induced defect generation in the amorphous phase is responsible for the light-induced degradation. In the following experiment, we investigate the behavior of the reverse bias enhanced degradation in nc-Si:H cells under different light spectra. Again, the red light was obtained using white light with a 665 nm cut-on filter, and the blue light with a 650 nm cut-off filter. During the light soaking, the blue and red light intensities were adjusted using a lens to produce the same J_{sc} as that under 100 mW/cm^2 of white light. The applied bias was –1.5 V, and the light-soaking time was 309 hours. The experimental results are listed in Table X. One can see that after soaking under red light, the solar cell does not degrade, which is the same as the result of light soaking under open circuit condition. Under blue light, the V_{oc} degrades by 30 mV, and FF by 7.9%, compared to 67 mV degradation in V_{oc} and 10.2% in FF under white light. Clearly, the white light causes more degradation than blue light under the reverse bias, which is different from that under open circuit condition.

Table X. J-V characteristics of the nc-Si:H single junction solar cells before (In.) and after (Deg.) light soaking with a reverse bias of –1.5 V at different light spectra. The light soaking was carried out at 50 ^{o}C for 309 hours. The intensities of the red, blue, and white lights were adjusted to produce the same short circuit current in the cells.

Cell No.	Light-soaking Conditions	Status	V_{oc} (V)	ΔV_{oc} (mV)	FF	$\Delta FF/FF_{in.}$ (%)
1	Red light	In.	0.472		0.593	
	-1.5 V	Deg.	0.472	0	0.598	+0.8
2	Blue light	In.	0.468		0.585	
	-1.5 V	Deg.	0.438	-30	0.539	-7.9
3	White light	In.	0.472		0.587	
	-1.5 V	Deg.	0.405	-67	0.527	-10.2

3.4.4 Light-assisted annealing in nc-Si:H solar cell degraded under reverse bias

As previously reported, the reverse bias enhanced light-induced degradation in the nc-Si:H solar cells can be annealed away at high temperatures, indicating a metastable defect generation similar to the Staebler-Wronski effect in a-Si:H. Although there is no observable room temperature recovery of the reverse bias enhanced light-induced degradation in the nc-Si:H cells in the dark, it can be partially recovered by subsequent light soaking under open circuit condition as shown in Fig. 12. In this experiment, two nc-Si:H solar cells from the same substrate were selected for exposure to 100 mW/cm^2 of white light at 50 ºC. One cell (referred to as cell 1) was light-soaked under open circuit condition throughout the whole procedure. The other cell (cell 2) was light-soaked under 2 V of reverse bias for 300 hours, and then the reverse bias was removed and the cell was subjected to the same light-soaking condition as cell 1 for the rest of the experiment. We find that for cell 2, during the first 300 hours of light soaking, the reverse bias caused a larger degradation in both FF and V_{oc}. The V_{oc} degrades by 16 mV, and FF by 11.1% in cell 2, as compared to the change of 7 mV and 3.6% in cell 1 that was degraded under open circuit condition. With the reverse bias being removed, the degradation in cell 2 was partially recovered, and cell 1 continued to degrade. Eventually, the two cells reached the same performance. This phenomenon is very similar to the light-soaking experiments under an initial higher light intensity and followed by a lower light intensity for a-Si:H solar cells. An enhanced degradation by a higher intensity light recovers, after a subsequent lower intensity illumination, to the value that is the same as obtained by a continuous lower intensity illumination [12-13].
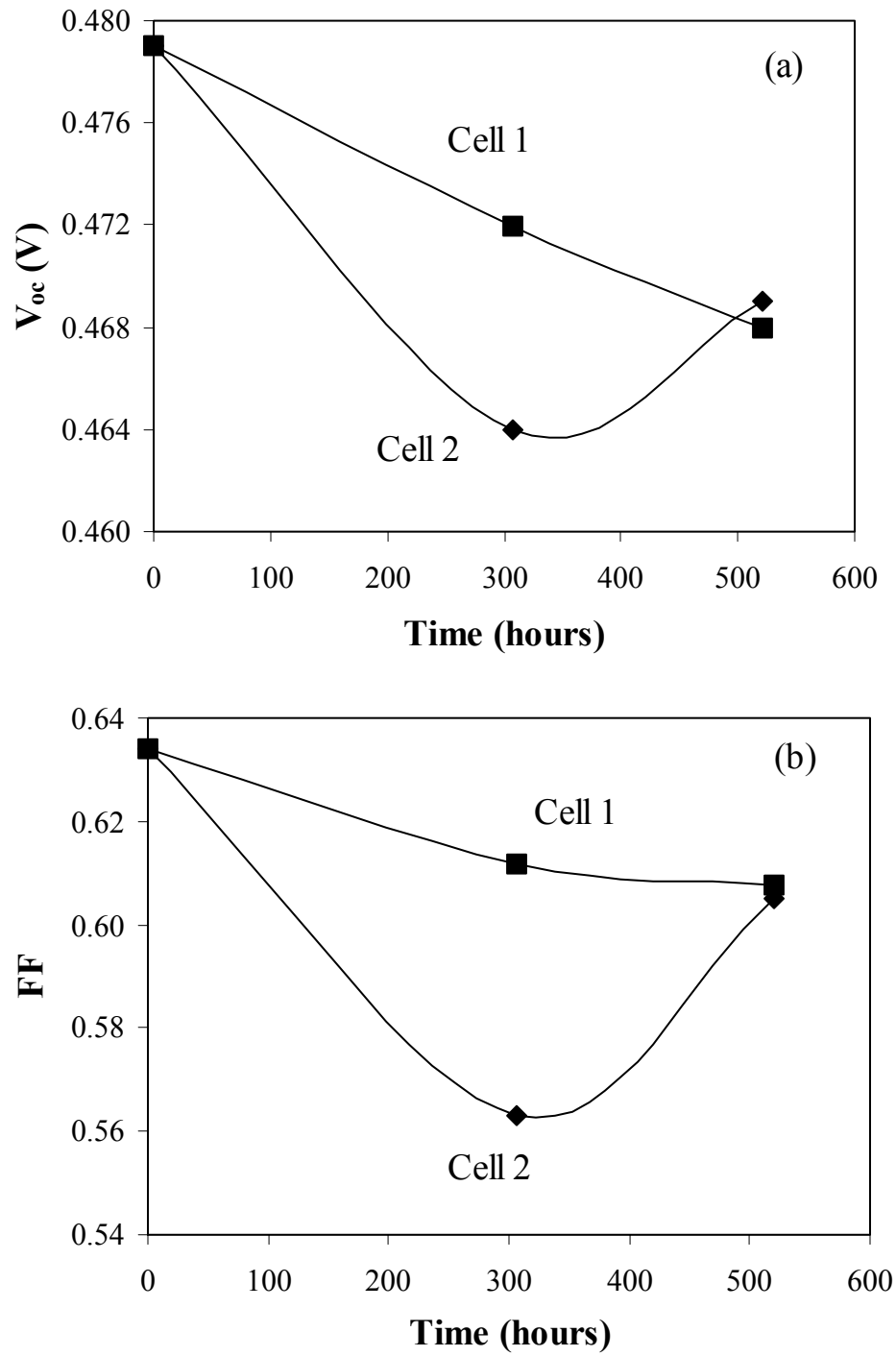
Figure 12. Photo-assisted annealing effect for the enhanced degradation by reverse bias. Cell 1 was light-soaked under open circuit condition throughout the whole procedure. For the first 300 hours, cell 2 was light-soaked under a reverse bias of 1 V, and then the reverse bias was removed. The solid line is only a guide for the eye.

22

4.4 Discussions

4.4.1 Back-to-Back connected diode model

Due to the complex heterogeneous structure, the transport of carriers in nc-Si:H solar cells is not very well understood. In general, nc-Si:H can be considered as a mixed material comprised of grains and amorphous tissues. Based on transmission electron microscopy (TEM) and atomic force microscopy (AFM) [14,15], Kočka *et al.*[17] proposed a model of nc-Si:H structure including large grain boundary and large grains with aggregation of tightly packed small grains. The small grains have a diameter of a few nanometers to over 20 nanometers. At the initial growth, the small grains are isolated from each other and embedded in amorphous tissues. The initial layer with a low nanocrystalline volume fraction is normally called incubation layer and is avoided for solar cell deposition [17]. With the film growing thick, the crystalline volume fraction increases. As a result, the small grains aggregate to form large grains and the amorphous tissues form narrow layers called large grain boundaries in the picture proposed by Kočka *et al.* [16]. Based on this model, most of the transport properties of nc-Si:H can be explained [16] assuming that the large grain boundaries are characterized by a wide bandgap with band tail states and the large grains have a narrow gap with bandtail states. The band tails in the large grains are from the grain boundary states. This model is also used to explain the defect structure in nc-Si:H films measured by electrically detected electron spin resonance [18], where two types of silicon dangling bonds are identified.

Based on the structure proposed by Kočka *et al.* [16], we now discuss possible mechanisms to explain the observed phenomena. Due to the nature of columnar growth of large grains, it is easy to form a percolation transport path of crystalline phase along the growth direction. In the dark, the conductivity in the amorphous phase (corresponding to large grain boundary region with Kočka's notation [16]) is much lower than that in the crystalline phase (large grains). The diffused or injected current from the doped layers basically flows through the percolation path of the grains, and tunnels through the thin amorphous phase between two small grains. A previous experiment has shown that only the recombination events in the amorphous phase and grain boundaries are responsible for the degradation in nc-Si:H cells [11]. Since there are no excess carriers in the amorphous phase, current-induced degradation does not occur [9].

When exposed to light, the amorphous phase in the nc-Si:H material has to be considered because the conductivity of the amorphous and nanocrystalline phases becomes comparable. In the current path including the amorphous phase, the material is a randomly distributed hetero-junction system formed by an amorphous phase and large grains, which have different bandgaps and activation energies. Considering a given amorphous region, if both sides are large grains with a low bandgap, the interface region between the amorphous and grains can form a microscopic diode. Thus, a small unit of 'crystalline-amorphous-crystalline' is equivalent to two microscopic back-to-back connected diodes [8]. If we further assume that the nanocrystalline grains are more n-type material than the amorphous phase, the electrons will be accumulated in the amorphous side, and the crystalline side is depleted of electrons and accumulates holes when they form a diode. The charge redistribution will create a local internal electric field at the boundary between the amorphous and nanocrystalline phases. In this case, the conduction and valence bands of the amorphous side are bent down, and the conduction and valence bands of the crystalline side are bent up. To illustrate this picture, a schematic band diagram of a 'crystalline-
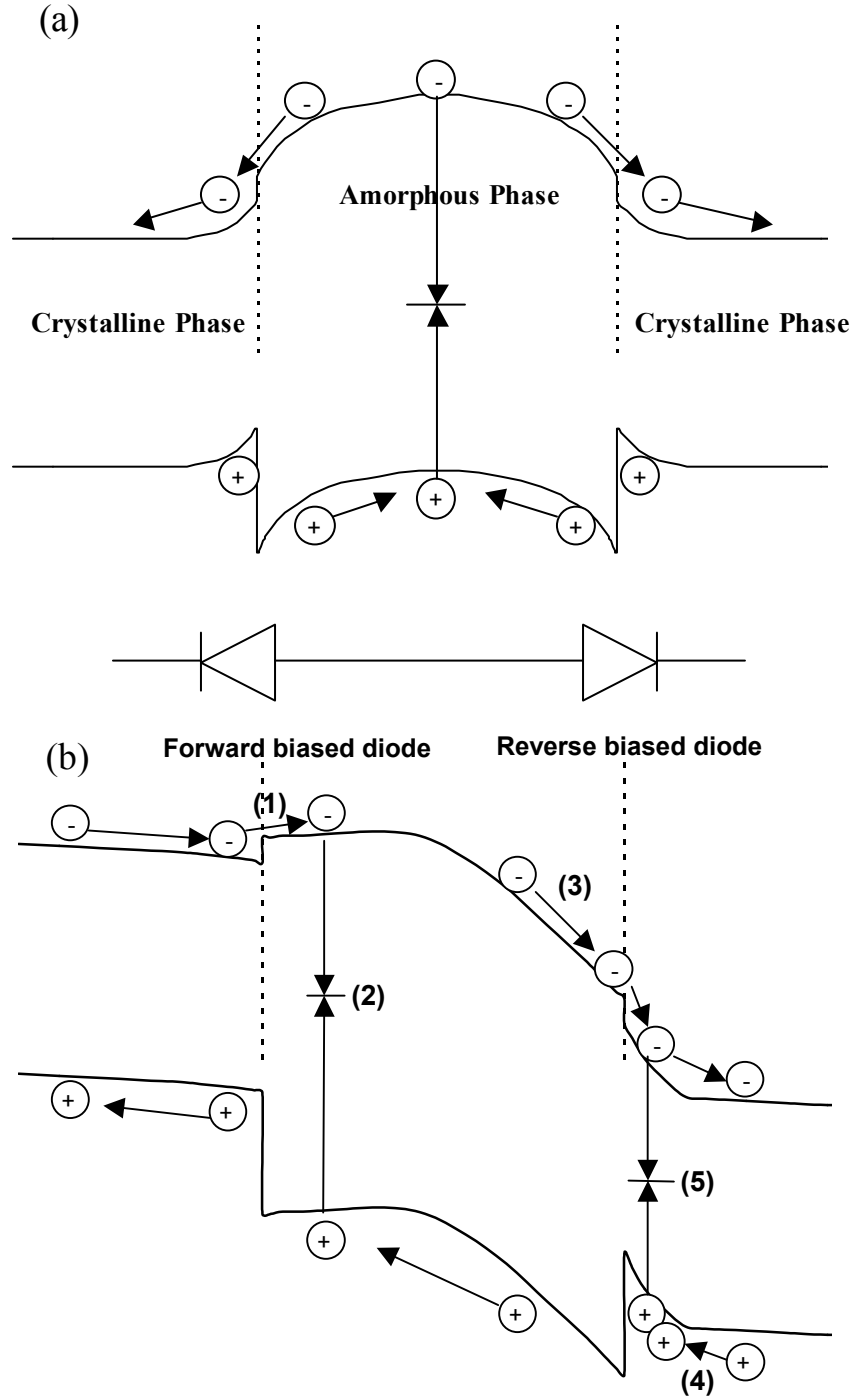
Figure 13. The band diagram of a 'crystalline-amorphous-crystalline' region in nc-Si:H material to illustrate the back-to-back diode model. (a) is under open circuit and (b) is under reverse bias during light soaking. In (b), (1) represents the electron injection into the amorphous phase from the left crystalline phase in the forward biased diode; (2) photo-generated electron-hole pairs recombine in the forward biased region of the amorphous phase; (3) photo-generated electrons are swept out of the reverse biased region in the amorphous phase by an electric field; (4) holes accumulate in the grain boundary in the right crystalline region; and (5) electrons recombine with the accumulated holes in the grain boundary region.

amorphous-crystalline' region is drawn in Fig. 13, where (a) corresponds to the open circuit condition and (b) to the condition under a reverse bias. One can see that the excess electrons in the amorphous phase generated by illumination have a tendency to move out of the amorphous phase and into the grain boundary region, where they will recombine with the holes accumulated in the crystalline side. Therefore, we expect that in addition to the light-induced defect generation in the amorphous region, light-induced defects would also be generated in the grain boundary region. In reality, there may not be a clear boundary between the amorphous and crystalline phase. With a finite thickness of the grain boundary region, the defect generation in the grain boundary region could play a significant role in carrier transport and solar cell performance. In addition, the grain boundary region may have much higher defect density than the ordinary a-Si:H. Based on this picture, it is not difficult to imagine that the light-induced degradation in nc-Si:H solar cells depends not only on the properties of the amorphous phase, such as the amorphous volume fraction, but also on the grain boundary properties, such as the hydrogen concentration and the structure of chemical bonds.

4.4.2 Explanation for the experimental results

When a reverse bias is applied to a nc-Si:H cell, the band diagram of the 'crystalline-amorphous-crystalline' structure is as shown in Fig. 13 (b). In this case, there are two mechanisms that give rise to the enhanced degradation of nc-Si:H cell performance. First, for the forward biased diode (left side in Fig. 13 (b)), photo-generated electrons in the crystalline regions will move towards the amorphous regions. These excess electrons together with the electrons generated in the amorphous region will recombine with the holes generated in the amorphous region as illustrated by (1) and (2) in Fig. 13 (b). This will increase the defect generation rate in this region. However, on the right side, the enhanced electric field would sweep out the excess electrons more efficiently, which is similar to the reverse-biased light soaking on conventional a-Si:H solar cells, where the light-induced degradation is significantly suppressed by reverse bias. The internal field distribution within the amorphous region will determine whether there will be net additional defects created by the application of reverse bias or not. This in turn is determined by the thickness of these regions and also the nature of the boundaries between the amorphous and the nanocrystalline phase. If the thickness is small and the internal field is high, defect generation would take place only in the forward biased region (when a reverse bias is applied). The field in the rest of the region would be sufficiently high to prevent recombination either in the open circuit or the reverse bias case. Thus, there will be more light-induced defects generated by the application of an external reverse bias than when no bias is applied. In addition, we need to consider the second process as illustrated by (3), (4), and (5) in Fig. 13 (b). The excess electrons generated in the amorphous phase would easily move out of the amorphous phase on the right side of the figure. However, the electric field drives a significant amount of photo-generated holes in the crystalline region to the grain boundary as illustrate by (4), and the excess electrons moved to the grain boundary region will recombine with holes there as described by process (5). It would be logical to assume that the grain boundary region has poor structure and more hydrogen concentration. Therefore, the recombination at the grain boundary will enhance the total defect generation. To summarize the proposed back-to-back diode model, we believe that two processes can cause the enhanced light-induced degradation by a reverse bias: First, the reduced electric field in the forward-biased diode causes addition recombination in the corresponding region. Second, the electrons driven

out of the amorphous region by electric field in the reverse diode recombine with the accumulated holes in the grain boundaries, which also produce additional defects.

An immediate challenge for this model is that why a forward external bias does not increase the light-induced degradation. First, it is difficult to apply a high forward bias without damaging the solar cell. For example, a 0.48 V of forward bias corresponds to the open circuit condition. Second, a forward bias causes a significant current injection and the injected space charges make the bias voltage drop mainly at the *p/i* interface region. In the bulk of the intrinsic layer, the electric field would be unaffected. Therefore, it is reasonable that no measurable difference was found between light-induced degradation under forward bias and open circuit conditions.

The results of the quantum efficiency loss and color fill factor measurements (as shown in Figs. 10 and 11) suggest that the light-induced degradation in the nc-Si:H cells is not uniform. As we have mentioned earlier, FF_r is a measure of hole transport whereas FF_b is governed by electron transport. Since the mobility of electrons is higher than that of holes, one would in general expect less degradation in FF_b than in FFr. When a forward bias is applied, however, the potential drop across the *p-i* interface would reduce the field there, resulting in significant recombination at that interface. Since the blue photons generate carrier only near that interface, it is apparent that FF_b would show a larger degradation under forward bias than FF_r. The reverse bias enhanced degradation under different light spectra also provides additional supports for the model illustrated in Fig. 13. Under red light, most of the photons are absorbed in the nanocrystalline phase, and there are no photo-generated carriers in the amorphous phase. The resistance of the amorphous phase is still much higher than the nanocrystalline phase. Thus, the percolation path through the nanocrystalline grains is still the dominant current path. Although there might be a charge accumulation on both sides of the amorphous phase, the recombination rate would not be expected to increase dramatically. Consequently, no light-induced degradation occurs. On the other hand, for the blue light, most of the photons are absorbed in the amorphous phase close to the *p-i* interface since the absorption coefficient in the short wavelength region is much higher than in the crystalline phase. Recombination takes place both at the interface and in the bulk. Bulk recombination should have the same bias dependence as discussed earlier with reverse bias inducing more recombination. Interface recombination, however, is reduced under reverse bias. For blue light the ratio of carriers generated at the interface to those in the bulk is larger than that for white light illumination. The overall degradation under reverse bias for blue light soaking would thus be less than that for white light soaking. The light-assisted annealing of the enhanced degradation by the reverse bias is very similar to the light-assisted annealing in a-Si:H, a phenomenon that was originally observed in material properties such as photoconductivity and defect density, and later on in a-Si:H solar cell performance [12, 13]. A simple rate equation including a light-induced annealing term can explain the recovery of the defect created under some extreme conditions such as very high light intensity or pulsed light illumination, but cannot explain the continued degradation after the light-induced annealing. The concept of 'fast' and 'slow' defects was proposed [10] to explain these results where the two defect states have different annealing rates. In general, light-induced defects have a continuous distribution of annealing activation energies. Therefore, the phenomena as shown in Fig. 12 could be simply explained by a continuous distribution of annealing activation energy [19]. However, we believe that there is more physics behind the phenomenon. As discussed above, nc-Si:H has a complicated structure and it should be logical to assume that there are more than one type of defects. Lips *et. al.* [18] have detected two kinds of silicon dangling bonds using

electrically detected electron spin resonance. In our case, one might assume that the defects generated in the amorphous phase are different from those in the grain boundary region. If two kinds of defects have different generation rates and annealing activation energies, one could interpret the results of Fig. 12 as explained for the light-assisted annealing in a-Si:H solar cells [12,13].

4.5 <u>Summary and Conclusion</u>

We have studied the behavior of light-induced degradation in nc-Si:H solar cells under various electrical bias conditions. We found that there is no forward-current-induced degradation in the dark, but an enhanced light-induced degradation under reverse bias. This is contrary to the results obtained in a-Si:H cells. Moreover, a forward bias does not cause additional light-induced degradation in the cell performance compared to the case of open circuit condition. The color FF and quantum efficiency loss measurements show that the light-induced defects generated under reverse bias are different from those under open circuit condition in terms of affecting the solar cell performance. The nc-Si:H cells light-soaked under reverse bias show significant degradation on the long wavelength response and in FF_r. The effect of reverse bias on the light-induced degradation is more pronounced for illumination with white light than blue light. In addition, the enhanced light-induced degradation by reverse bias can be partially annealed away at the same temperature under the same illumination, but under open-circuit condition. Based on the experimental results, we propose a model to interpret the reverse bias enhanced light-induced degradation in nc-Si:H solar cells. We believe that a 'crystalline-amorphous-crystalline' region in the nc-Si:H layer could be considered as a back-to-back connected diode structure. Considering the recombination at the *p-i* interface, in the amorphous silicon region, and at the grain boundaries, we explain most of the experimental observations using the proposed model in a self-consistent manner.

References

[1] A. Banerjee and S. Guha, J. Appl. Phys. **69**, 1030 (1991).

[2] B. Yan, G. Yue, J. Yang, S. Guha, D. L. Williamson, D. Han, and C.-S. Jiang, Appl. Phys. Lett. **85**, 1599 (2004).

[3] B. Yan, G. Yue, A. Banerjee, J. Yang, and S. Guha, Mater. Res. Symp. Proc. **808**, 581 (2004).

[4] G. Ganguly, T. Ikeda, K. Kajiwara, and A. Matsuda, Mater. Res. Soc. Symp. Proc. **467**, 681 (1997).

[5] T. Matsui, A. Matsuda, and M. Kondo, Mater. Res. Soc. Symp. Proc. **808**, 557 (2004).

[6] J. Yang, K. Lord, B. Yan, A. Banerjee, and S. Guha, Mater. Res. Soc. Symp. Proc. **715**, 601 (2002).

[7] S. Klein, F. Finger, R. Carius, B. Rech, L. Houben, M. Luysberg, and M. Stutzmann, Mater. Res. Soc. Symp. Proc. **715**, 617 (2002).

[8] R.E.I. Schropp, Y. Xu, E. Iwaniczko, G.A. Zaharias, and A.H. Mahan, Mater. Res. Soc. Symp. Proc. **715**, 623 (2002).

[9] G. Yue, B. Yan, J. Yang, and S. Guha, Proc. of 31st IEEE Photovoltaic Specialist Conference, (Florida, Jan. 2005), in press.

[10] A. Banerjee, X. Xu, J. Yang, and S. Guha, Appl. Phys. Lett. **67**, 2975 (1995).

[11] B. Yan, G. Yue, J. M. Owens, J. Yang, and S. Guha, Appl. Phys. Lett. **85**, 1925 (2004).

[12] L. Yang and L. Chen, Mater. Res. Soc. Symp. Proc. **297**, 619 (1993).

[13] X. Xu, J. Yang, and S. Guha, Mater. Res. Soc. Symp. Proc. **297**, 649 (1993).

[14] E. Vallat-Sauvain, U. Kroll, J. Meier, A. Shah, and J. Pohl, J. Appl. Phys. **87**, 3137 (2000).

[15] J. Bailat, E. Vallat-Sauvain, L. Feitknecht, C. Droz, and A. Shah, J. Appl. Phys. **93**, 5727 (2003).

[16] J. Kočka, A. Fejfar, H. Stuchlílová, J. Stuchlík, P. Fojtík, T. Mates B. Rezek, K. Luterová, V. Švrček, and I. Pelant, Sol. Energy Mater. Sol. Cells **78**, 493 (2003).

[17] B. Yan, G. Yue, A. Banerjee, J. Yang, and S. Guha, Mater. Res. Symp. Proc. **762**, 309 (2003).

[18] K. Lips, P. Kanschat, and W. Fuhs, Sol. Energy Mater. Sol. Cells **78**, 513 (2003).

[19] B. Yan, J. Yang, K. Lord, and S. Guha, Mater. Res. Symp, Proc. **664**, A25.2 (2001).